A.C.S. Dallas

DE89 011240

CONF-890401--10

Decomposition of Incomplete Fusion

L.G. Sobotka, D.G. Sarantites, D.W. Stracener, Z. Majka,[a]
V. Abenante and T.M. Semkow[b]

Department of Chemistry, Washington University,
St. Louis, Missouri 63130

D.C. Hensley, J.R. Beene and M.L. Halbert

Oak Ridge National Laboratory, Oak Ridge, Tennessee 37830

ABSTRACT

The velocity distribution of fusion-like products formed in the reaction 701 MeV $^{28}Si+^{100}Mo$ is decomposed into 26 incomplete fusion channels. The momentum deficit of the residue per non-evaporative mass unit is approximately equal to the beam momentum per nucleon. The yields of the incomplete fusion channels correlate with the Q-value for projectile fragmentation rather than that for incomplete fusion. The backward angle multiplicities of light particles and heavy ions increase with momentum transfer, however, the heavy ion multiplicities also depend on the extent of the fragmentation of the incomplete fusion channel. These data indicate that at fixed linear momentum transfer, increased fragmentation of the unfused component is related to a reduced transferred angular momentum.

The decline of the complete fusion cross section in heavy ion reactions as the relative velocity at contact exceeds 1/10 c is well known. The telltale sign of this decline is found in measurements of the velocity distributions of the fusion-like residues (ER)[1] or in measurements of the angle between fission fragments.[2] In the former case the velocity distributions are broad and skewed to low velocities with mean values less than expected for complete momentum transfer. Coarsely, one can divide the explanations for this incomplete momentum transfer into those where the projectile nucleons carrying the non-fusing momentum traverse the target nucleus, and those where they do not. The latter, most appropriate for large impact parameters, was first provided by the sum rule model

---

[a]Permanent address: Institute of Physics, Jagellonian University, Krakow, Poland.

[b]Permanent address: Wadsworth Center for Laboratories and Research, New York State Department of Health, Albany, NY 12201.

of Wilczynski.[3] Here the projectile fragments into two pieces, one which fuses and the other which continues on a Coulomb trajectory with a velocity close to that of the beam. In this model, the nonfusing mass provides a crude impact parameter selection. On the other hand, for small impact parameters, one must account for incomplete fusion by lack of sufficient stopping power to thermalize the relative kinetic energy within the nuclear volume. Pre-equililbrium models of this sort have taken several forms, including Fermi jets,[4,5] hotspot formation[6,7] and the standard pre-equilibrium model[8] modified for heavy-ion systems.[9] More recently, Harvey has generated a model based on free nucleon-nucleon scattering.[10] This model may be valid over a broad range of impact parameters, but is undoubtedly restricted to high energy heavy-ion collisions due to the lack of an explicit treatment of Pauli bocking. Another recent and promising development is the melding of the Fermi jet model to the nucleon exchange model developed for lower energy deep inelastic heavy-ion collisions.[11] The relevance of the different mechanisms underlying these models is one of the fundamental issues in the study of intermediate energy heavy-ion reactions. This is so, not simply because we wish to understand why complete fusion ceases to be viable, but also because of the restrictions imposed by these mechanisms on our capabilities of forming and therefore studying highly excited and rapidly rotating nuclear systems.

In this work we take a large step towards a complete experimental documentation of the nature of the incomplete fusion process. This is accomplished by decomposing the velocity distribution of fusion-like products, formed in the reaction 701 MeV ^{28}Si+^{100}Mo, into channels specified by the exclusive charge (Z_f) and mass (A_f) which compose the fast forward spray of particles for each event. The relative probabilities for these channels correlates with the Q-value for projectile fragmentation rather than the Q-value for the overall incomplete fusion reaction. The channels are further characterized by the backward angle multiplicity of neutrons, γ-rays and charged particles. The forward angle particle data and the velocity of the residue are used to determine the decrement in the linear momentum transferred to the fusion-like product per forward non-evaporative mass unit. The backward angle data show that while the multiplicities increase with increasing momentum transfer, they also depend on the extent of the fragmentation of the mass in the channel definition. Specifically, backward angle

heavy ion emission is strongly suppressed when the incomplete fusion channel is highly fragmented.

This study required a multi-layered coincidence apparatus capable of detecting all of the emissions associated with fusion-like events. These include: a) the evaporation residue; b) the nonfusing components which, as stated above, specify the channel and c) the products which result from the de-excitation of the highly excited, rapidly rotating, compound system (mostly n, p, α and γ's). These diverse needs are served by a detection scheme incorporating: a) a forward annular parallel plate avalanche counter (PPAC) spanning 2.1° to 8.1° in the laboratory; b) a forward wall of 35 plastic-CsI scintillators subtending angles between approximately 11° and 35°; and c) a small ball of 64 plastic-CsI scintillators subtending angles larger than approximately 35°, which is positioned inside a large multielement NaI ball. This experiment was done at the HHIRF facility at Oak Ridge National Laboratory, where the 72 element NaI Spin Spectrometer[12] was used to detect the γ-rays and neutrons. In this work, the most forward NaI elements were removed in order to make room for an enlarged scattering chamber to house the CsI Wall and the PPAC. Therefore, only 65 of the 72 Spin Spectrometer elements were used, corresponding to 88% of 4π. The plastic-CsI multidetector system, which we call the Dwarf Ball and Wall, utilizes the different time characteristics of scintillation output, the phoswich technique. An early version of this device,[13] along with one of the important subsequent modifications,[14] is described in the literature. For the present study, each plastic-CsI module provides light charged particle identification (LCP= p, d, t and α), distinguishes these LCP's from heavy ions (HI) and provides an energy for the LCP's. The energy calibration for LCP was obtained from elastic and inelastic proton scattering on ^{12}C at two bombarding energies.

We have identified 26 channels differing by their forward light charged particle composition. These channels consist of 1, 2, 3 and 4 LCP's. The ER velocity distributions are shown in Fig. 1 for selected channels and the sum of all charged particle channels. The latter distribution should be quite similar to the inclusive distribution (omitting only xn channels) and the most probable velocity, 77% of the full momentum transfer value, is consistent with the systematics presented in Ref. 1. These distributions can be understood as consisting of two parts. One of these components, which arises from the detection of all the forward

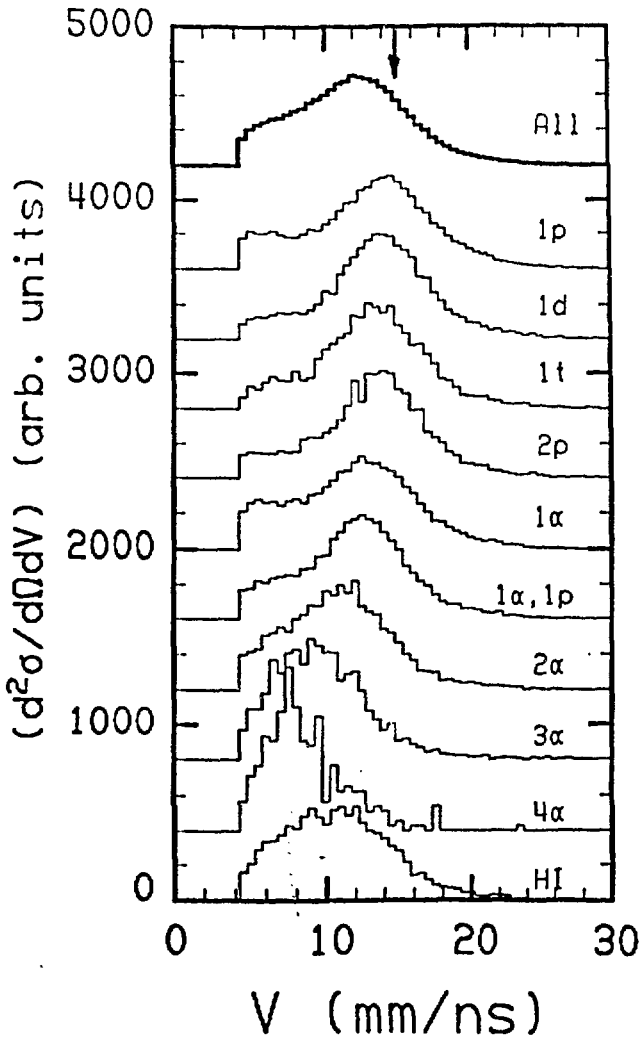

Figure 1. The channel decomposition of the velocity distribution of fusion-like products. The channels are labeled by the type and number of the forward particles. The top (bold) distribution is the sum of all charged particle channels. The distributions are offset from the abscissa for display. The arrow indictes V_{full}.

light charged particles, takes the form of a gaussian at the higher velocities. On the other hand, if some forward particle is not detected, as would occur for $\theta_{LCP} < 11°$, then the channel is misidentified. The latter case produces a background distribution peaked at lower ER velocities, i.e., lower values of the momentum transfers. In order to extract both the channel probablity and the mean ER velocities for each channel, we transform the velocity distributions to a Galilean invariant representation and fit the large V_{ER} portion by a gaussian.

The centroids of these fits divided by the velocity values expected for full momentum transfer, $R = V/V_{full}$, are shown in Fig. 2. It should be emphasized that these ratios are channel selected and independent of the extent of sequential evaporation. The latter quality originates from the use of Galilean invariant cross sections.[1] (Formally, a $\cos\theta$ term should exist in the denominator of the ratio; however the small angles used in the present study make this correction negligible.)

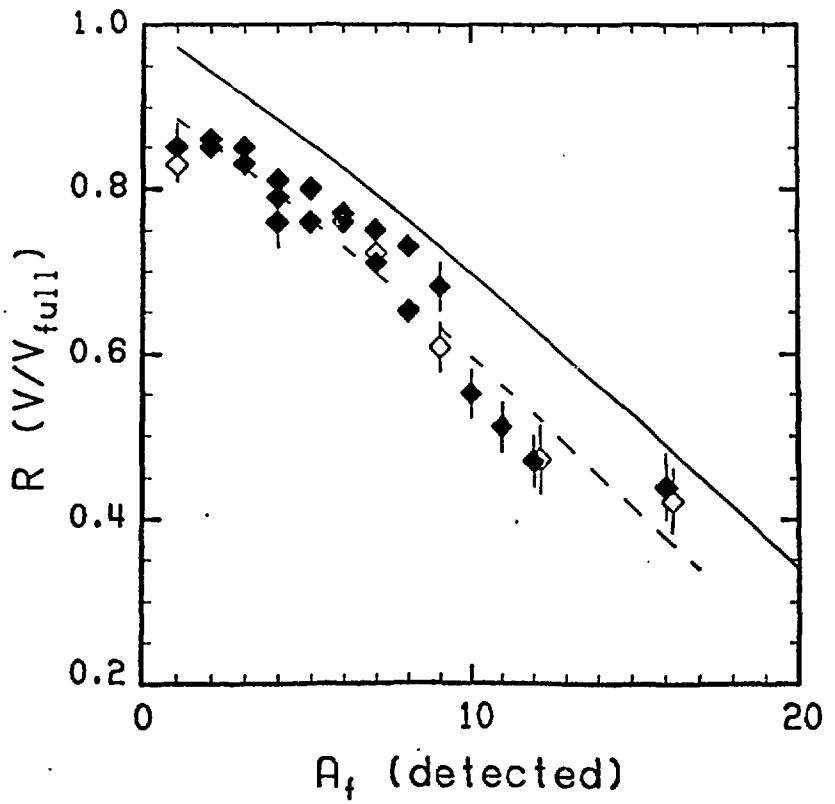

Figure 2. Ratio of velocity centroid of the channel selected data to the value for complete momentum transfer. The abscissa (A_f) corresponds to all detected forward mass (solid diamonds) and to the detected forward mass with energies greater than the evaporation peak (open diamonds). The solid line is the result of a calculation assuming a linear momentum deficit equal to $A_f\times$ the beam momentum per nucleon. The dashed curve assumes 3 additional beam velocity nucleons (neutrons) exist in each channel but are not observed.

Figure 2 can be used to determine the mean linear momentum per nucleon associated with the forward particles which compose our channel definition. The solid line is the expected residue velocity if, on average, each of the A_f nucleons has the beam momentum per projectile nucleon, P_0/A_p. These data exhibit the same slope as the solid line, indicating that on average each nucleon included on our channel definition results in a linear momentum transfer deficit equal to the beam momentum per nucleon. The downward displacement of these data can be explained by the fast forward neutrons which are not counted in the channel definition, A_f. D. Hilscher *et al.*[15] have determined the number of non-evaporative neutrons as a function of momentum transfer in the reaction 30 MeV/nucleon Ne+Ho.[15] Their results indicate that there are between 2 and $3\frac{1}{2}$ pre-equilibrium neutrons for linear momentum transfers between 50% and 100%. Applying the average correction implied by this result shifts the solid line in Fig. 2, to the left 3 mass units and yields the dashed line. Close inspection of Fig. 2, and the associated channel compositions, indicates that it is the multiple α-particles in the channel definition which determines the overall trend. More decomposed channels tend to have a slightly larger residue volocity or momentum transfer per nucleon.

These conclusions could be influenced by an underlying evaporative component in our channel definition. To estimate the magnitude of this contamination, we have done single component moving source fits to the backward ($\theta_{Lab} > 75°$) LCP data. The velocity of the source was fixed to the centroid values of narrow residue velocity bins (ΔV = 2mm/ns for $V < V_{full}$). Extrapolation of these fits to forward angles provides an estimate of the evaporative contamination in our channel definition. At most, 40% of the protons, 30% of the α-particles and smaller fractions of the deuterons and tritons selected in the forward Wall can be the result of isotropic evaporation from the residue. In order to reduce the evaporative component in the channel definition, we have obtained distributions similar to those shown in Fig. 1 with the requirement that all particles in the channel definition not only be forward of 35°, but also have energies in excess of the evaporation peak. Representative points obtained from the gaussian fits of the Galilean invariant representations of these distributions are shown as open symbols in Fig. 2. The trend of the data is unaltered, verifying that, on the average, each non-evaporative forward nucleon is responsible for a deficit in the

momentum transfer equal to the beam momentum per nucleon. This analysis retains the effect of particle energy correlations on the momentum transfer (or ER velocity) which is lost in analyses based solely on the inclusive particle energy spectra.

TABLE I

Channel Yields

Channel	Energy Integrated (%)	Energy Truncated (%)
p	17.4	17.2
d	7.0	11.1
t	4.0	6.8
α	19.7	26.9
p p	5.1	2.4
p α	11.4	7.6
α α	7.1	6.6
α α α	1.6	1.0
α α α α	.2	?
p d	4.1	3.1
p t	2.5	2.3
d d	$< .1$	?
d t	.9	1.2
d α	4.8	5.2
t α	2.7	3.1
p p α	2.9	.9
p α α	3.5	1.4
p d α	2.4	1.2
d d α	.5	.4
d α α	1.4	1.1
t α α	.8	.5

The yields of the identified channels are listed in Table I. As done for the velocity centroids, two methods where used to extract these yields. Energy

integrated channels yields are given in the second column and the yields of channels where each particle in the channel definition has an energy in excess to the evaporation peak are shown in the third column.

The standard picture of incomplete fusion[3] is that of a one step process where the probabilities are related to the cost of creating the final state, given by the overall Q-value.

$$M_{projectile} + M_{target} => M_{ch} + M_{target+transfered} + Q_{fusion} \qquad (1)$$

However, our channel data indicate that there is only a weak correlation between this Q-value and the yields. This is shown in Figure 3a, where the relative yields are plotted versus this fusion Q-value. The squares are the total energy integerated values while the diamonds represent the truncated integration, columns 2 and 3 in Table I respectively. On the other hand, the yields do correlate with the projectile fragmentation Q.

$$M_{projectile} => M_{ch} + M_{transfered} + Q_{fragmentation} \qquad (2)$$

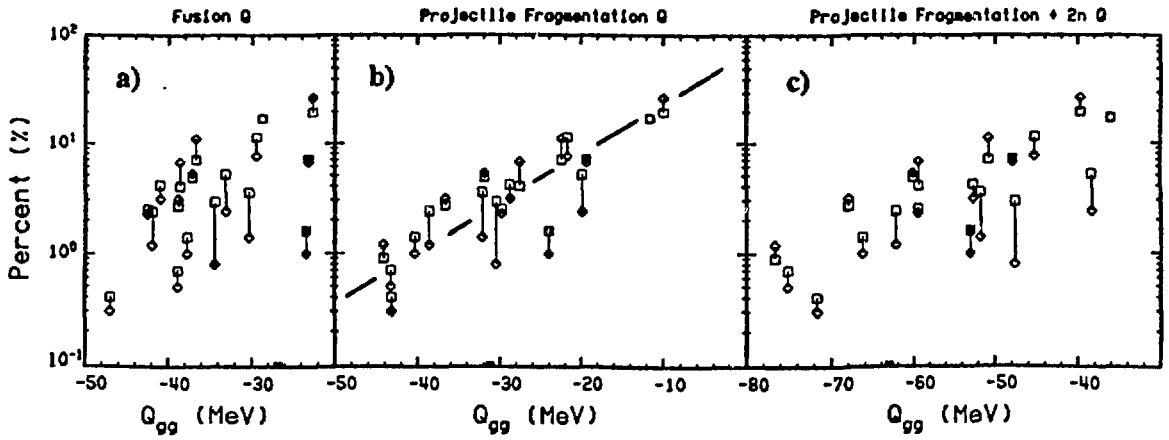

Figure 3. Correlation between channel probablity and Q-value. Channels defined by all forward particles irregardless of kinetic energy are represented by squares. Channels defined only by particles with energies in excess of the evaporation peak are represented by diamonds. The solid symbols are for the 2α, 3α, and 4α channels. Table I contains a list of the channels. The abscissa for a) is the Q-value for incomplete fusion (eq. 1), b) is the Q-value for projectile fragmentation (eq. 2), and c) is the Q-value for projectile fragmentation with 2 additional free neutrons.

Figure 3b demonstates this feature. The improvement in the correlation in going from Q_{fusion} to $Q_{fragmentation}$ can be traced to the fact that with increasing mass transfer the binding energy per nucleon of the target + transfered component decreases (eq. 1) while the opposite is true of the projectile remanant which is the transfered component (eq. 2).

Stokstad et al. have shown that projectile fragmentation reactions do in fact exhibit the type of correlation seen in fig 3b.[16] This prompts us to suggest that incomplete fusion proceeds by a two step process, a projectile disassembly followed by partial fusion, in which the cost of the first step determines the yields. This concept is different than that of Wilczyński's sum rule model.[3] The relevance of the fragmentation Q in our reaction while the incomplete fusion Q seems to determine the yields in the 10 MeV/nucleon ^{14}N + ^{159}Tb reaction studied in ref 3, may be due to the difference in beam energies and/or to the more highly fragmented nature of our channels.

The forward ($\theta_{Lab} < 35°$) and backward ($\theta_{Lab} > 35°$) charged particle multiplicities M_x as a function of the percentage momentum transfer, ρ, are shown in Figs. 4a and b, respectively. (The fictitious values of $\rho > 100\%$ arise from the random nature of the evaporation sequence which can boost $V > V_{full}$.) The open symbols correspond to the inclusive residue-charged particle coincidences while the solid symbols correspond to the specific channels; see below.

The inclusive, non-channel selected multiplicities in the backward direction increase with increasing ρ and tend to saturate as full momentum transfer is approached. (The heavy ion multiplicities saturate at smaller values of the momentum transfer than do the light ion multiplicities. This behavior can be understood as a result of the greater sensitivity of the heavy ion decay to angular momentum. This is discussed below.) This dependence indicates that the multiplicity of charged particles at large angles is a measure of the violence of the collision in the same fashion as has been previously demonstrated for the neutron multiplicity[15] and as we have also found from the present study, (see Fig. 5). The same cannot be said of the forward multiplicities. These reflect the momentum transfer itself, and therefore there is a slight enhancement of $M_{z=1}$ for relatively large values of ρ, while M_α and M_{HI} peak at low values of ρ. The *total* forward charged particle multiplicity is rather insensitive to momentum transfer, and therefore cannot be used as an indicator of the centrality or violence of the

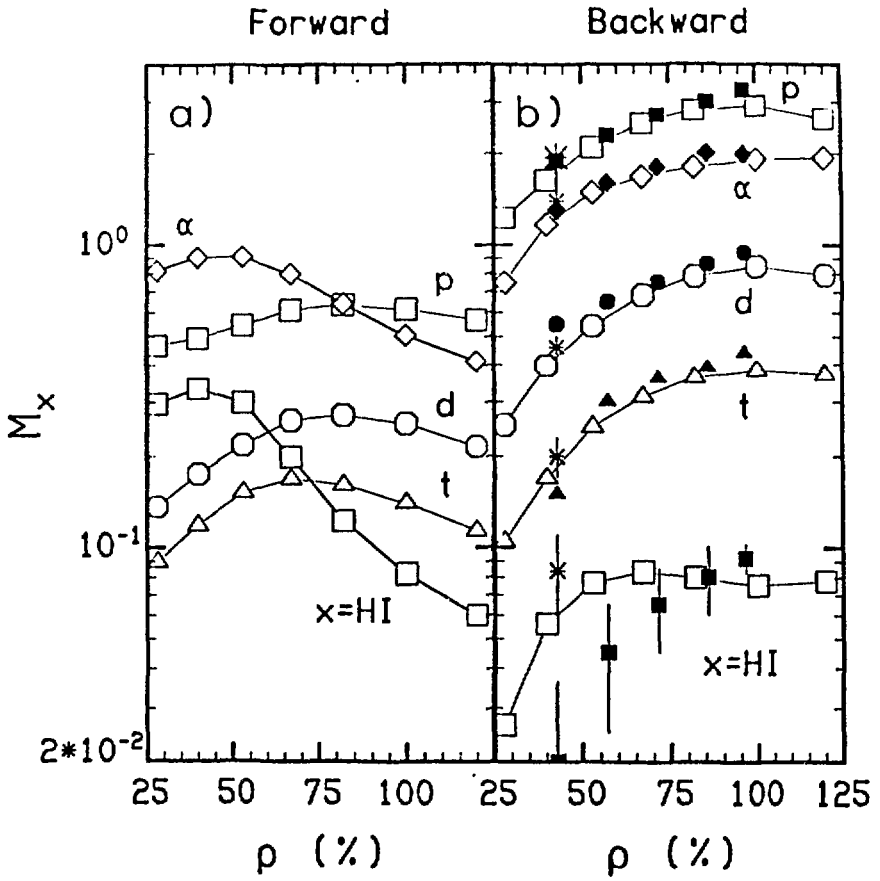

Figure 4. The multiplicities of charged particles detected at a) forward ($\theta < 35°$) and b) backward ($\theta > 35°$) angles as a function of the linear momentum transfer. The open symbols are derived from inclusive charged particle-residue coincidences. The solid and star symbols are derived from a subset of the inclusive data where specific exclusive channels (forward particles) are selected, see text.

collision. This has also been found to be true in the study of the reactions ^{36}Ar + ^{238}U at $E/A = 35$ MeV and ^{14}N + ^{238}U at $E/A = 50$ MeV.[17]

The solid points in Fig. 4b are the backward multiplicities (M_p, M_α, M_d, M_t and M_{HI}) for the specific incomplete fusion channels, $1p$, 1α, 2α, 3α and 4α with decreasing ρ. At the five values of ρ corresponding to these channels, the solid points represent a subset of data represented by the open points. An additional subset for small ρ is shown by stars which show the backward multiplicities for the HI channel with the same momentum transfer as for the 4α channel. For the most part, these channel selected multiplicities agree with each other and the inclusive values. The exceptions are the values of M_{HI} for small ρ. As most of the excitation energy of the fused system is dispensed in the form of neutrons,

protons and α-particles, the agreement between the values of M_p and M_α for the channel selected and inclusive data indicates that the value of ρ prescribes a value of the excitation energy.

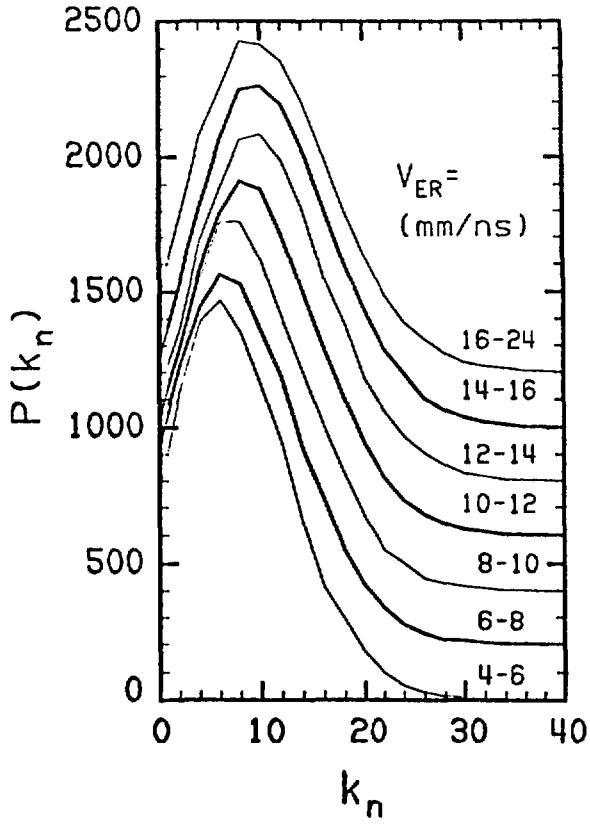

Figure 5. Neutron fold distributions for seven residue velocity bins. These distributions are deduced from the backward, $\theta_{lab} > 75°$, NaI detectors with an overall solid angle correction to account for the solid angle with $\theta_{lab} < 75°$. The distributions are offset from the abscissa for display.

If the mean excitation energies of the emitting nuclei in the channel selected and inclusive data are the same, there must be a difference between the angular momentum distributions to account for the difference in HI evaporation. Since HI evaporation is known to be far more sensitive to angular momentum than is light particle evaporation[18] and HI evaporation is suppressed for the 3α and 4α channels (the solid points at $\rho = 57\%$ and 43%, respectively) then the transferred spin for these channels must be less than the transferred spin for other channels contributing to the same region of ρ. This is verified by selecting the HI channel, stars in Fig. 3. While the total excitation energy is virtually the same as the 4α

channel and the inclusive data (see M_p and M_a), the M_{HI} is significantly larger than that arising from the 4α channel. This indicates that the highly fragmented incomplete fusion channel transfers less angular momentum than does a channel with an intact spectator.

The influence of angular momentum is not only observed in the channel dependence of the HI multiplicity but also in the overall dependence of M_{HI} on momentum transfer. As pointed out earlier, M_{HI} increases faster at low ρ and saturates sooner than do the M_{LI} data. This can be explained by the combined influence of increasing excitation energy and generally decreasing angular momentum transfer with increasing ρ. On the other hand light ion evaporation reflects the strictly increasing E with increasing ρ.[18]

Previous experimental studies have investigated the relationship between linear and angular momentum transfer.[19,20] The present work demonstrates that, for fixed linear momentum transfer, the angular momentum transfer depends on the nature of the incomplete fusion channels. It is possible to reconcile this observation with the standard model of incomplete fusion[3] by applying the critical angular momentum (ℓ_{cr}) condition for fusion to each exit channel fragment rather than to the entrance channel. The application of ℓ_{cr} logic to the exit channel of binary systems has previously been suggested in order to explain transferred spins, deduced from γ-ray multiplicity measurements, which are less than those calculated from the entrance channel condition even allowing for angular momentum fractionation.[21,22] Consider the case where the ^{27}Si breaks up into ^{16}O and ^{12}C and the ^{12}C fragment fuses, (see inset on the right hand side of Fig. 6). The critical angular momentum condition applied to the ^{16}O – target $+^{12}$C system indictes that all total angular mementa less than 40 $\hbar$ will fuse. On the other hand, if the ^{16}O breaks up into 4 alpha particles, only α – target $+^{12}$C systems with $\ell \lesssim 15\hbar$ will fuse, (see inset on the left hand side of Fig. 6). (Here we have ignored the perturbation caused by the other fragments. As long as they are light particles our qualitative argument is valid.) In other words, due to the fact that ℓ_{cr} decreases with increasing mass asymmetry, light fragments can escape from smaller impact parameter collisions than can large fragments. This allows fragmented channels to exist in a region of impact parameters or total ℓ-waves not allowed to non-fragmented channels.

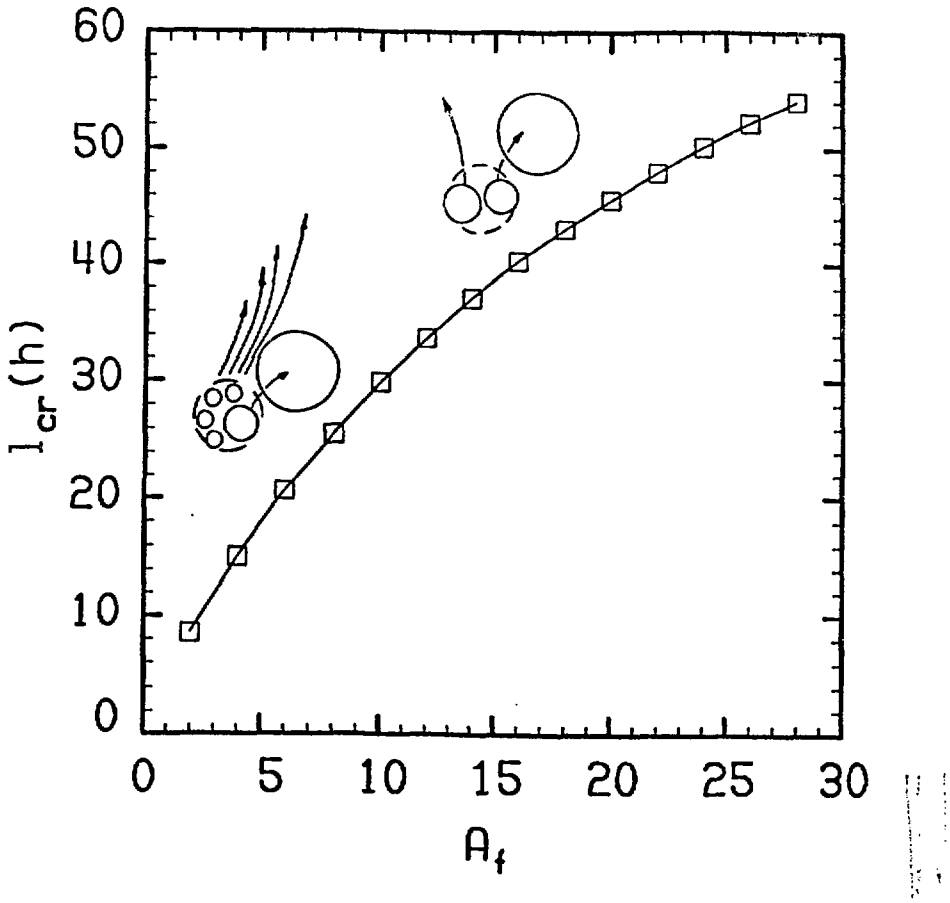

Figure 6. The critical angular momentum values for the ^{28}Si + ^{100}Mo system as a function of exit channel mass asymmetry. In this calculation the remainder of the projectile fuses. The values of ℓ_{cr} are almost identical if the remainder of the projectile is neglected, presumed not to fuse.

In summary, we have made a channel decomposition of incomplete fusion. In doing so, we have shown that the yields of incomplete fusion channels correlate with the Q-value for projectile fragmentation rather than that for the total Q-value for the incomplete fusion. This suggests that incomplete fusion proceeds by a two step process. The first being the fragmentation of the projectile and it is the cost of this step which determines the channel probabilities. The difference in the dependence of the backward light and heavy ion multiplicities with linear momentum transfer indicate that while the backward multiplicities of light ions are indicators of the excitation energy deposition, the backward heavy-ion

multiplicity reflects both excitation and angular momentum deposition. Futhermore, the channel dependence of the heavy ion multiplicities shows that while on average the linear momentum transfer is proportional to the mass transfer; the angular momentum transfer, at fixed linear momentum transfer, depends on the fragmentation of the unfused part of the projectile. This feature of incomplete fusion reactions can be understood by transferring the concept of the critical angular momentum for fusion from the entrance channel to the stage of the reaction following the fragmentation of the projectile.

Acknowledgements

This work is supported by U.S. Department of Energy under grants DE-FG02-87ER40316 and DE-FG02-88ER40406. One of us, L.G.S., acknowledges the support from a U.S. Presidential Young Investigator Award. Oak Ridge National Laboratory is operated by Martin Marietta Energy Systems, Inc, under contract DE-AC05-84OR21400.

REFERENCES

1. H. Morgenstern *et al., Phys. Rev. Lett.* 52, 1104 (1984), and Y. Chan *et al., Proceedings of the International Symposium on the Many Facets of Heavy-Ion Fusion Reactions,* Argonne, 1986, Argonne National Laboratory Report ANL-PHY-86-01, 1986, p. 219.
2. K. Kwiatkowski *et al., Nucl. Phys.* 471, 271c (1987).
3. J. Wilczyński *et al., Phys. Rev. Lett.,* 45, 606 (1980) and J. Wilczyński *et al., Nucl. Phys. ,* A373, 109 (1982).
4. J.P. Bondorf *et al, Nucl. Phys.,* A333, 285 (1980).
5. K. Möhring, W.J. Świątecki and M. Zielińska-Pfabé, *Nucl. Phys.,* A440, 89 (1985).
6. H.A. Bethe, *Phys. Rev.,* 53, 675 (1938).
7. R. Weiner and M. Westrõm, *Nucl. Phys.,* A286, 282 (1977).
8. G.D. Harp, J.M. Miller and B.J. Berne, *Phys. Rev.,* 165, 1166 (1968).
9. M. Blann, *Phys. Rev.,* C31, 1245 (1985).
10. B.G. Harvey, *Nucl. Phys.,* A444, 498 (1985).
11. J. Randrup and R. Vandenbosch, *Nucl. Phys.,* A474, 219 (1987).
12. M. Jääskeläinen *et al., Nucl. Instru. Meth.,* 204, 385 (1983).
13. D.G. Sarantites *et al., Nucl. Instru. Meth.,* A264, 319 (1988).
14. E. Norbeck, T. Dubbs and L.G. Sobotka, *Nucl. Instru. Meth.,* A262, 546 (1987).
15. D. Hilscher, *Nucl. Phys.,* A471, 77c (1987).
16. J. Pouliot *et al., Phys. Lett.,* in press and Lawrence Berkeley Laboratory Report, LBL-26768 (1989).
17. M.B. Tsang *et al., Phys. Lett.,* in press (1989).
18. L.G. Sobotka *et al., Phys. Rev.,* C36, 2713 (1987).
19. N.M. Namboodiri *et al., Phys. Rev.,* C35, 149 (1987).
20. K. Hagel *et al., Nucl. Phys.,* A486, 429 (1988).
21. W. Dünnweber *et al., Phys. Rev. Lett.* 52, 1405 (1984).
22. Z. Majka *et al.,* submitted for publication, Washington University Preprint (1989).